

RESEARCH ARTICLE

Vascular Biology and Microcirculation

Soluble epoxide hydrolase deletion attenuated nicotine-induced arterial stiffness via limiting the loss of SIRT1

Shuiqing Hu,^{1,2} Jinlan Luo,³ Menglu Fu,³ Liman Luo,³ Yueting Cai,^{1,2} Wenhua Li,³ Yuanyuan Li,³ Ruolan Dong,⁴ Yan Yang,⁵ Ling Tu,^{2,3} and Xizhen Xu^{1,2}

¹Division of Cardiology, Department of Internal Medicine, Tongji Hospital, Tongji Medical College, Huazhong University of Science and Technology, Wuhan, People's Republic of China; ²Hubei Key Laboratory of Genetics and Molecular Mechanisms of Cardiological Disorders, Wuhan, People's Republic of China; ³Department of Geriatric Medicine, Tongji Hospital, Tongji Medical College, Huazhong University of Science and Technology, Wuhan, People's Republic of China; ⁴Institute of Integrated Traditional Chinese and Western Medicine, Tongji Hospital, Tongji Medical College, Huazhong University of Science and Technology, Wuhan, China; and ⁵Division of Endocrinology, Department of Internal Medicine, Tongji Hospital, Tongji Medical College, Huazhong University of Science and Technology, Wuhan, China

Abstract

Arterial stiffness, a consequence of smoking, is an underlying risk factor of cardiovascular diseases. Epoxyeicosatrienoic acids (EETs), hydrolyzed by soluble epoxide hydrolase (sEH), have beneficial effects against vascular dysfunction. However, the role of sEH knockout in nicotine-induced arterial stiffness was not characterized. We hypothesized that sEH knockout could prevent nicotine-induced arterial stiffness. In the present study, *Ephx2* (the gene encodes sEH enzyme) null (*Ephx2*^{−/−}) mice and wild-type (WT) littermate mice were infused with or without nicotine and administered with or without nicotinamide [NAM, sirtuin-1 (SIRT1) inhibitor] simultaneously for 4 wk. Nicotine treatment increased sEH expression and activity in the aortas of WT mice. Nicotine infusion significantly induced vascular remodeling, arterial stiffness, and SIRT1 deactivation in WT mice, which was attenuated in *Ephx2* knockout mice (*Ephx2*^{−/−} mice) without NAM treatment. However, the arterial protective effects were gone in *Ephx2*^{−/−} mice with NAM treatment. In vitro, 11,12-EET treatment attenuated nicotine-induced matrix metalloproteinase 2 (MMP2) upregulation via SIRT1-mediated yes-associated protein (YAP) deacetylation. In conclusion, sEH knockout attenuated nicotine-induced arterial stiffness and vascular remodeling via SIRT1-induced YAP deacetylation.

NEW & NOTEWORTHY We presently show that sEH knockout repressed nicotine-induced arterial stiffness and extracellular matrix remodeling via SIRT1-induced YAP deacetylation, which highlights that sEH is a potential therapeutic target in smoking-induced arterial stiffness and vascular remodeling.

arterial stiffness; nicotine; SIRT1; soluble epoxide hydrolase; vascular remodeling

INTRODUCTION

Tobacco use is widespread worldwide and the number of daily smokers has increased significantly since 1980 (1). Although cigarette smoking can increase arterial stiffness (2, 3), a potent risk factor of cardiovascular diseases (CVD), which has widespread detrimental implications for organ function (3, 4). Arterial stiffness, characterized by vascular extracellular matrix (ECM) remodeling, is associated with hypertension, stroke, and chronic kidney disease (3–5). Clearly, it is important to understand the mechanisms behind arterial stiffness and find a novel treatment approach.

Epoxyeicosatrienoic acids (EETs), synthesized by cytochrome P450 (CYP) enzymes, play an essential role in vascular

homeostasis, including vasodilation, vascular smooth muscle cell (VSMC) antimigratory actions, and anti-inflammatory actions (6–8). Soluble epoxide hydrolase (sEH) readily converts epoxides, including EETs, to less biological active diols (7). Smoking affects EETs levels and sEH activity, resulting in enhanced sEH activity and decreased plasma EETs levels (9). sEH inhibition and *Ephx2* deletion significantly attenuated smoking-induced pulmonary vascular dysfunction and inflammation (10–12). In addition, the possible synergism between the genetic role of EETs metabolism and environmental exposure of nicotine on vascular pathophysiology has been reported before (13). However, the functional role of EETs was not characterized in smoking-induced vascular stiffness.

Sirtuin-1 (SIRT1), a class III protein deacetylase, is found in the nucleus and cytosol with a massive range of roles in transcriptional regulation, energy metabolism modulation, cell survival, DNA repair, and anti-inflammation (14–16). Emerging data demonstrate that SIRT1 has protective effects in CVD by inhibiting VSMC destruction, endothelial dysfunction, vascular oxidative stress, and inflammation (15–17). It was reported that the expression and activity of SIRT1 were inhibited in nicotine-induced arterial stiffness (18). Moreover, SIRT1 activation can depress aortic stiffness in mice and humans (18–20). A recent study indicated that EETs attenuated ischemia/reperfusion-induced acute kidney injury by activating SIRT1 (21). Nevertheless, the relationship between SIRT1 and EETs in vascular stiffness was not explored.

In this study, we used *Ephx2*^{−/−} mice to study the potential role of sEH in nicotine-induced arterial stiffness. It was demonstrated that sEH knockout markedly inhibited nicotine-induced arterial stiffness via limiting the loss of SIRT1 expression, which then prevented yes-associated protein (YAP)-triggered matrix metalloproteinase 2 (MMP2) transcription.

MATERIALS AND METHODS

Study Approval

All animal care and experimental procedures were reviewed and approved by the Experimental Animal Research Committee of Tongji Medical College, Huazhong University of Science and Technology (Wuhan, China) and strictly complied with the *Guide for the Care and Use of Laboratory Animals* of the National Institute of Health (Bethesda, MD).

Materials and Reagents

The specific information of primary antibodies was presented in the major resources tables. Nicotine (n3876-25mL) was purchased from Sigma-Aldrich (St. Louis, MO). Nicotinamide (NAM) (Cat. No. HY-B0150) was purchased from Med Chem Express (MCE, Monmouth). Selisistat (Cat. No. EX527) was purchased from Selleck (Shanghai, China). 5,6-EET (Cat. No. 50211), 8,9-EET (Cat. No. 50351), 11,12-EET (Cat. No. 50511), 14,15-EET (Cat. No. 50651), 11,12-DHET (Cat. No. 51511), and 14,15-EEZE (Cat. No. 10004946) were purchased from Cayman Chemical (Ann Arbor, MI). 11,12-EET/DHET ELISA Kit (Cat. No. DH5/DH15/DH25/DH105) and 14,15-EET/DHET ELISA Kit (Cat. No. DH2) were purchased from Detroit R&D (Detroit, MI). DAB Detection Kit (Polymer) (Cat. No. GK600510) was purchased from Gene Tech (Shanghai, China). MMP Zymography Assay Kit (Cat. No. P1700) was purchased from Apply Gen (Beijing, China). The major resources tables can be found in the Supplemental Material at <https://doi.org/10.6084/m9.figshare.14566491.v2>.

Ephx2-KO Mice Generation

The *Ephx2*-KO mice were generated by the CRISPR/Cas9 technique. The gRNA (described in Table 1) was designed and transcribed in vitro and then injected into mouse fertilized eggs. The Cas9 protein binds to the target site under the

Table 1. The sequence of gRNA

Name	Sequence (5′-3′)	Pam
gRNA1	GCCTGGTGACCCATAGTATC	TGG
gRNA2	CTCTATTCGTCCTTAAA	TGG

guidance of gRNA, which caused DNA double-strand breakdown.

Animals and Treatment

Ephx2-KO mice (Cat. No. T011427) with C57BL/6J background were obtained from GemPharmatech (Nanjing, China). *Ephx2*-KO mice were genotyped by standard PCR using the following primers: TF1, 5′-CCCTCATGCTCACTGACTAGAAATG-3′; TR1, 5′-CAGTCGGTCTCTGCTGGATGT-3′; TF2, 5′-GCATTGTCACCAACAACCTGGCT-3′; and TR2, 5′-CTTTGTGAGTAACTCGGGCAGCT-3′. Primer TF1/TR1 yielded a 300-bp amplicon for the *Ephx2*-null allele, and primer TF2/TR2 yielded a 405-bp amplicon for the WT (wild-type) allele. PCR reactions were performed for each sample. The presence of both amplicons indicates an *Ephx2*^{+/−} mouse and a 405-bp amplicon only indicates a WT mouse. In addition, a 300-bp amplicon only indicates an *Ephx2*^{−/−} mouse.

Male *Ephx2*^{−/−} mice and WT littermate control mice were used in this study at 8-wk old. Mice were divided into six groups ($n = 6$ per group): 1) WT + vehicle (Veh), 2) WT + nicotine, 3) WT + nicotine + NAM, 4) *Ephx2*^{−/−}, 5) *Ephx2*^{−/−} + nicotine, and 6) *Ephx2*^{−/−} + nicotine + NAM. All mice were housed in a temperature-controlled room under a 12-h:12-h light/dark photoperiod, free access to drinking water and normal chow.

At the age of 8 wk, mice were infused with nicotine (5 mg/kg/day) or saline (0.9% sodium chloride) for 4 wk, using Alzet mini-osmotic pumps (Model 2004, DURECT Corporation, Cupertino, CA), according to the product instruction. Simultaneously, mice were administered with NAM (10 mg/kg/day) or PBS for 4 wk.

Pump Implantation Procedure

After anesthetizing and surgically preparing, we made a small incision in the skin at the mid-scapular region on the mouse back. Then we inserted a hemostat into the incision to separate the skin from the subcutaneous connective tissue to make a small pocket for the pump. After that, we inserted a pump with the delivery port inward and closed the incision.

Cell Culture and Treatment

Mouse aortic smooth muscle cells (Movas) purchased from American Type Culture Collection (ATCC) were cultured in DMEM medium (Gibco) containing 10% FBS. When cells grown to ~70% confluence in culture dishes, Movas were pretreated with or without EETs (10 μ M) for 2 h, followed by nicotine (1 μ M) accompanied with or without Selisistat (EX-527, 10 μ M), 14,15-EEZE (1 μ M), and 11,12-DHET (1 μ M) treatments for 24 h.

Enzyme-Linked Immunosorbent Assay

The levels of 11,12-DHET and 14,15-DHET in aortas were measured by ELISA according to the instruction. The sEH

activity (Cat. No. 10011671, Cayman Chemical), aortal SIRT1 activity (Cat. No. CS1040, Sigma-Aldrich), and plasma cotinine levels (Cat. No. QZ-12667, Jiu Bang) were also measured by ELISA according to the manufacturer's instructions.

Measurement of Aortic Pulse Wave Velocity

Aortic pulse wave velocity (PWV) was measured using a Vevo 2100 Imaging System (FUJIFILM, Visual Sonics, Toronto, ON, Canada). Before the test, mice were anesthetized with 1% isoflurane and placed on a heated (37°C) platform to maintain body temperature and monitor electrocardiogram (ECG) and heart rate (HR). Hair was removed using a depilatory agent (Veet). The B-mode was used to visualize the abdominal aorta and then M-mode was used to record aortic wall motion. Images were analyzed using the Vevo WorkStation. The aortic PWV was calculated as the distance between two measurement points divided by the wave form's time shift at the two points. At least three replicates were measured for each mouse.

Western Blot Analysis

At the end of the study, cultured cells were lysed by radioimmunoprecipitation assay (RIPA) lysis buffer containing protease inhibitors (Bimake, Cat. No. B14001, Houston, TX) for 30 min at 4°C and centrifuged at 12,000 g for 10 min. After removing the adventitia and endothelium, aortas were homogenized in RIPA lysis buffer with protease inhibitors on ice. The solution was centrifuged at 12,000 g for 10 min, and the liquid fraction was used for Western Blot analysis. Protein content was measured by the bicinchoninic acid (BCA) Protein Assay Kit (Boster Biological Technology, Cat. No. AR0146, CA). Protein (20 µg) was loaded onto an SDS-PAGE gel, electrophoresed, and then transferred to a polyvinylidene fluoride (PVDF) membrane. The membranes were blocked with 5% BSA for 2 h at room temperature and incubated with primary antibodies overnight at 4°C, followed by secondary antibodies conjugated with horseradish peroxidase for 2 h at room temperature. Protein bands were visualized by an ECL Plus chemiluminescence detection system reagent (Boster Biological Technology, Cat. No. AR1191). The bands were quantified and analyzed with ImageJ software (<http://rsb.info.nih.gov/ij/>).

Immunofluorescence Assay

For immunofluorescent staining, cross sections of aortas were deparaffinized, rehydrated, and repaired the antigens. Also, we used an autofluorescence quenching kit (Vector Laboratories, Cat. No. SP-B400, Burlingame) to remove the autofluorescence. Slides of cells were fixed with 4% paraformaldehyde for 20 min and permeabilized with 0.5% Triton X-100 for 10 min. The sections and cells were blocked with 5% BSA for 2 h at room temperature and incubated with primary antibodies overnight at 4°C, followed by fluorescent secondary antibodies for 2 h at room temperature. In addition, the nucleus was labeled with 4',6'-diamidino-2-phenylindole dihydrochloride (DAPI) (Servicebio, Cat. No. GDP1024, Wuhan, China). Images were generated by ZEN 2.1 software (Carl Zeiss, Oberkochen, Germany) and analyzed with Image-Pro Plus software (Media Cybernetics, Rockville, MD).

Morphological and Immunohistochemical Analysis

All aortas were harvested, fixed in 4% paraformaldehyde, embedded in paraffin, and 5-µm cross sections were prepared. Sections of slides were stained with Masson's Trichrome and Verhoeff's Van Gieson (EVG) using standard methods. We also performed immunohistochemical (IHC) staining by using DAB Detection Kit to detect protein expression (collagen I, fibronectin, SIRT1, sEH, MMP2, and pYAP). All the sections were examined under the same conditions and analyzed with Image-Pro Plus software (Media Cybernetics, Rockville, MD).

Immunoprecipitation

Movas or aortas lysates were prepared and incubated with protein A/G-agarose bead (Bimake, Cat. No. B23201, Houston, TX), bound with captured antibody, overnight at 4°C with gentle rotation. Immunoprecipitates were washed with wash buffer for three times and subjected to SDS-PAGE electrophoresis, followed by specific antibodies [SIRT1, YAP, pYAP, or acetyl-lysine (Ack)] incubation.

Gelatin Zymography

We used an MMP Zymography Assay Kit to assess matrix metalloproteinase (MMP) activity. The experiment was carried out according to the product manual. In short, samples were loaded onto 8% acrylamide gels containing 0.1% gelatin and electrophoresed (20 mA/gel, 3 h). After that, the gels were washed twice by wash buffer for 48 h and then incubated with developing cushion overnight at 37°C, followed by Coomassie brilliant blue staining for 2 h at room temperature. After decolorization and photographing, the bands were analyzed with ImageJ software.

siRNA Transfection

When the confluence reached ~70%, YAP siRNA (Ribobio, Guangzhou, China) was transfected into Movas by using Lipofectamine 2000 (Invitrogen) according to the product instruction. After 6 h, the medium was refreshed and Movas were treated with or without 11,12-EET (10 µM) for 2 h, followed by nicotine (1 µM) treatment for 66 h.

Statistical Analysis

All the quantitative results were presented as the means ± SD. We used the Student *t* test for unpaired observations to determine significant differences between two groups and a one-way ANOVA test to identify the differences among three or more groups, and two-way ANOVA test to determine the significant differences between grouped data with two variables. All the data were analyzed with GraphPad Prism 7.0 software (GraphPad Software, CA). *P* < 0.05 was considered statistically significant.

RESULTS

Nicotine Infusion Induced Arterial Stiffness with sEH Upregulation and Activation in Aortas

Male mice were infused with nicotine by the osmotic pump for 4 wk to simulate smoking-induced vascular stiffness. As cotinine, the metabolite of nicotine, is a marker of smoking state, we measured the plasma cotinine levels to

confirm nicotine administration (22, 23). As shown in Supplemental Fig. S1A, nicotine administration significantly increased the plasma cotinine levels, which were not affected by *Ephx2* deletion or NAM administration. In addition, aortic pulse wave velocity (PWV) (Fig. 1A) was measured to assess vascular stiffness. Compared with the vehicle group, nicotine treatment caused higher arterial PWV. Also, nicotine treatment upregulated the expression of MMP2, a critical molecule in ECM remodeling, in aortas (Fig. 1, B and C). These data indicated that nicotine administration induced arterial stiffness.

The expression of sEH in arteries, measured by immunoblotting (Fig. 1, B and D) and immunohistochemical (IHC) analysis (Fig. 1, E and F), was markedly upregulated in mice with nicotine-induced arterial stiffness. Moreover, the activity of sEH in aortas of nicotine-treated mice was also higher than that in vehicle-treated mice, as shown in Fig. 1G. These data indicated that sEH expression and activity were enhanced in mice with nicotine-induced arterial stiffness.

Ephx2 Knockout Prevented the Development of Nicotine-Induced Arterial Stiffness via Attenuating the Loss of SIRT1

EETs, hydrolyzed by sEH, have beneficial effects against vascular dysfunction. We generated *Ephx2*^{-/-} mice to explore the role of sEH in nicotine-induced arterial stiffness. Male *Ephx2*^{+/-} mice were mated with female *Ephx2*^{+/-} mice and then generated *Ephx2*^{-/-} mice and WT littermate mice, as shown in Fig. 2A. As indicated in Fig. 2B, genotypes of mice were identified by PCR, a 300-bp amplicon for the *Ephx2*-null allele was yielded with primer TF1/TR1 and a 405-bp amplicon for the WT allele was

yielded with primer TF2/TR2. Compared with WT mice, the expression of sEH in aortas, determined by IHC (Fig. 2, C and D) and Western Blot (Fig. 2, E and F), was decreased in *Ephx2*^{-/-} mice. Taken together, these data indicated that *Ephx2*^{-/-} mice and their littermate WT mice were successfully generated.

To further characterize the role of sEH in nicotine-induced arterial stiffness, *Ephx2*^{-/-} mice and WT mice were infused with PBS or nicotine (Fig. 3A). Compared with WT mice, *Ephx2*^{-/-} mice had lower arterial PWV (Fig. 3B) under nicotine administration. In addition, nicotine treatment decreased 11,12-EET levels in aortas of WT mice but not in *Ephx2*^{-/-} mice (Fig. 3C). Furthermore, we performed additional experiments to explore sEH protein levels (Fig. 3D and Fig. 4, G and N), sEH activity (Supplemental Fig. S1B), and other metabolites (Fig. 3, G–J). Nicotine treatment significantly increased sEH expression and activity and DHET level in WT mice, but not in *Ephx2*^{-/-} mice. Interestingly, *Ephx2* deletion and nicotine administration did not affect the generation of EETs, which indicates that sEH upregulation may be the key point in nicotine-induced arterial stiffness. Moreover, *Ephx2* knockout repressed nicotine-induced ECM remodeling characterized by decreased elastin fragmentation (Fig. 4, B and I) and collagen accumulation (Fig. 4, A, C, D, H, J, and K). Furthermore, *Ephx2* deletion attenuated nicotine-induced MMP2 upregulation (Figs. 3E and 4, E and L) and activation (Supplemental Fig. S2). Interestingly, nicotine administration also dramatically decreased SIRT1 expression and activity, which was markedly inhibited by *Ephx2* deletion (Figs. 3F and 4F, and Supplemental Fig. S3).

As *Ephx2* deletion attenuated nicotine-induced SIRT1 downregulation, we explored whether SIRT1 was involved

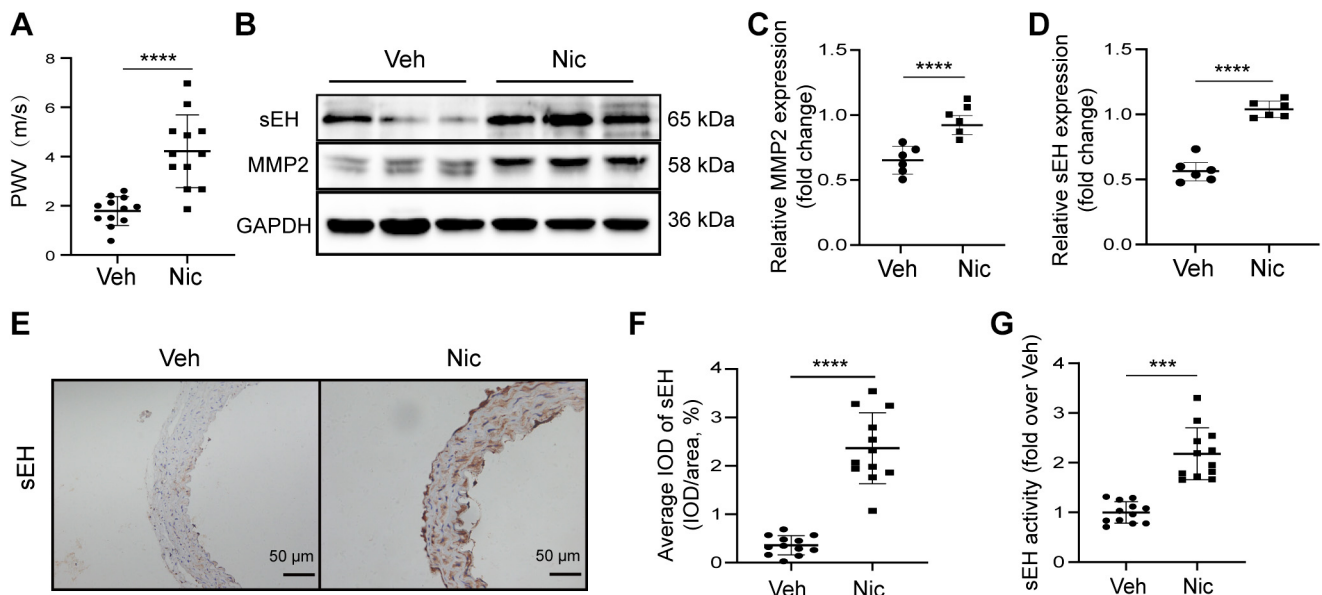


Figure 1. Nicotine-induced arterial stiffness with enhanced soluble epoxide hydrolase (sEH) expression and activity. A: analysis of arterial stiffness of abdominal aortas in vehicle- or nicotine-treated mice ($n = 12$). Representative images (B) and quantification of matrix metalloproteinase 2 (MMP2) (C) and sEH (D) expression in aortas based on Western Blot analysis from vehicle- or nicotine-treated mice ($n = 6$). Representative images (E) and quantification (F) of sEH in aortas based on immunohistochemical (IHC) staining of vehicle- or nicotine-treated mice ($n = 12$, scale bar = 50 μ m). G: analysis of sEH activity of abdominal aortas in vehicle- or nicotine-treated mice by ELISA ($n = 12$). Data are shown as means \pm SD by Student t test. *** $P < 0.001$; **** $P < 0.0001$. Nic, nicotine; Veh, vehicle.

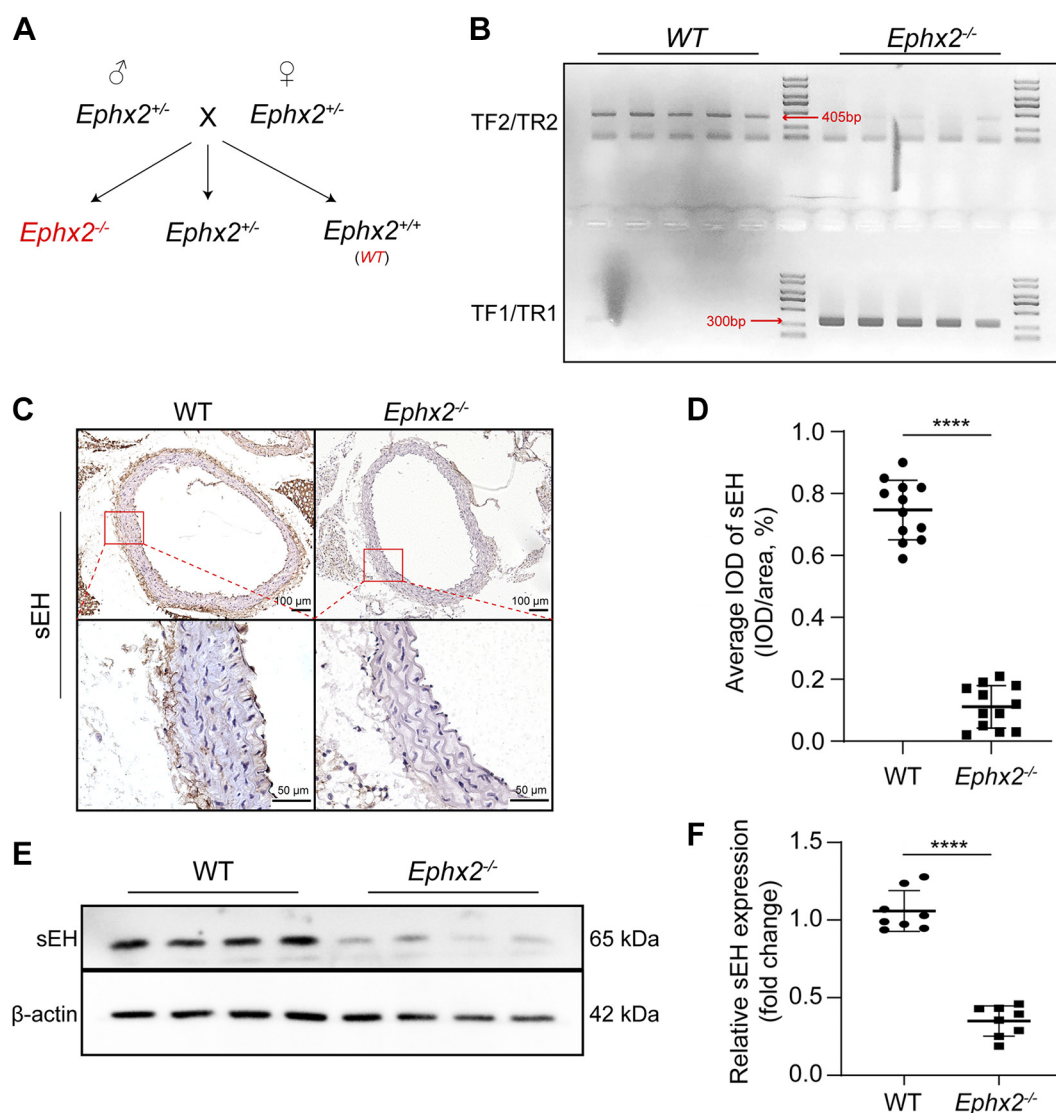


Figure 2. The generation of $Ephx2^{-/-}$ mice. **A:** schematic representation for the generation of $Ephx2^{-/-}$ mice and wild-type (WT) littermate mice. **B:** PCR analysis of genotype from mice tails. Representative images (**C**) and quantification (**D**) of soluble epoxide hydrolase (sEH) in aortas based on immunohistochemical (IHC) staining of $Ephx2^{-/-}$ mice and WT littermate mice ($n = 12$). Western Blot analysis (**E**) and quantification (**F**) of sEH expression in aortas of $Ephx2^{-/-}$ mice and WT littermate mice ($n = 8$). Data are shown as means \pm SD by Student t test. **** $P < 0.0001$.

in this process that $Ephx2$ deletion inhibited nicotine-induced arterial stiffness and ECM remodeling. $Ephx2^{-/-}$ mice and WT mice were treated with nicotine (5 mg/kg/day), and coadministered with or without NAM (nicotinamide, 10 mg/kg/day), a specific and efficient inhibitor of SIRT1, for 4 wk. As expected, NAM treatment significantly decreased SIRT1 expression and activity in both WT mice and $Ephx2^{-/-}$ mice under nicotine administration (Fig. 5B and Supplemental Fig. S3). Compared with $Ephx2^{-/-}$ mice, SIRT1 inhibition-attenuated $Ephx2$ knockout triggered beneficial effects in arterial remodeling characterized by high arterial PWV (Fig. 5A), increased elastin fragmentation (Fig. 5, F and K), increased accumulation of collagen (Fig. 5, E and J), and the upregulation of collagen I (Fig. 5, G and L), fibronectin (Fig. 5, H and M), and MMP2 (Fig. 5, C, I, and N). These data indicated that $Ephx2$ knockout markedly inhibited nicotine-induced

arterial stiffness via limiting the loss of SIRT1, whereas $Ephx2$ deletion alone did not enhance SIRT1 activation (Supplemental Fig. S3), which means that EETs may attenuate the decline of SIRT1 induced by nicotine administration.

11,12-EET Attenuated Nicotine-Induced MMP2 Upregulation via Limiting the Loss of SIRT1 Expression in Vitro

sEH readily converts EETs to their corresponding diols. To further explore the model epoxy lipid in nicotine-induced vascular stiffness, we used EETs to pretreat Movas, followed by nicotine treatment (Fig. 6A). Western Blot analysis indicates that 11,12-EET had the most potent effects in attenuating nicotine-induced MMP2 upregulation and SIRT1 downregulation (Fig. 6, B–D), which can be blocked by 14,15-EEZE (EET-antagonist) (Fig. 6, H and

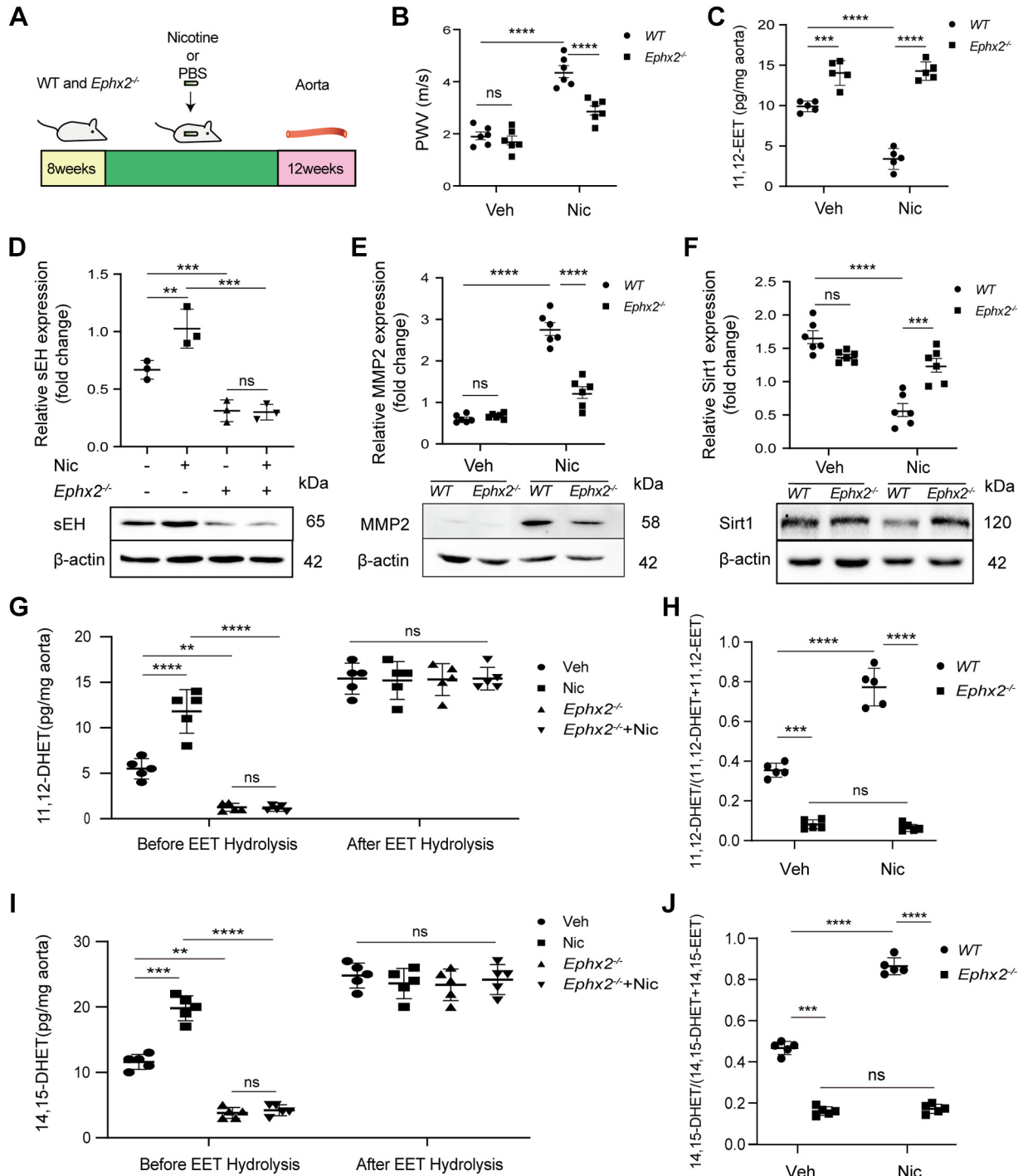


Figure 3. Soluble epoxide hydrolase (sEH) knockout attenuated nicotine-induced arterial stiffness and sirtuin-1 (SIRT1) downregulation. **A:** schematic representation of experimental protocol. **B:** analysis of arterial stiffness of abdominal aortas in *Ephx2*^{-/-} mice and wild-type (WT) mice treated with vehicle or nicotine for 4 wk (*n* = 6). **C:** analysis of 11,12-EET levels in abdominal aortas by ELISA from *Ephx2*^{-/-} mice and WT mice treated with vehicle or nicotine for 4 wk (*n* = 6). Western Blot analysis and quantification of sEH (**D**), MMP2 (**E**), and SIRT1 (**F**) expression in aortas from *Ephx2*^{-/-} mice and WT mice treated with vehicle or nicotine for 4 wk (*n* ≥ 3). **G:** analysis of 11,12-DHET levels in aortas by ELISA (*n* = 5). **H:** the ratio of 11,12-DHET/(11,12-DHET + 11,12-EET) (*n* = 5). **I:** analysis of 14,15-DHET levels in aortas by ELISA (*n* = 5). **J:** the ratio of 14,15-DHET/(14,15-DHET + 14,15-EET) (*n* = 5). All data are presented as means ± SD by two-way ANOVA. ***P* < 0.01; ****P* < 0.001; *****P* < 0.0001; ns, no significance.

I). In contrast, SIRT1 inhibition partially blocked these effects of 11,12-EET on MMP2 and SIRT1 expression (Fig. 6, E–G). Interestingly, 11,12-DHET administration did not worsen nicotine-induced MMP2 upregulation (Fig. 6, H and I).

Ephx2 Knockout Attenuated Nicotine-Induced YAP Activation via SIRT1-Mediated Deacetylation

The enhanced activation of YAP, a critical molecular in ECM remodeling, was reported in nicotine-induced vascular

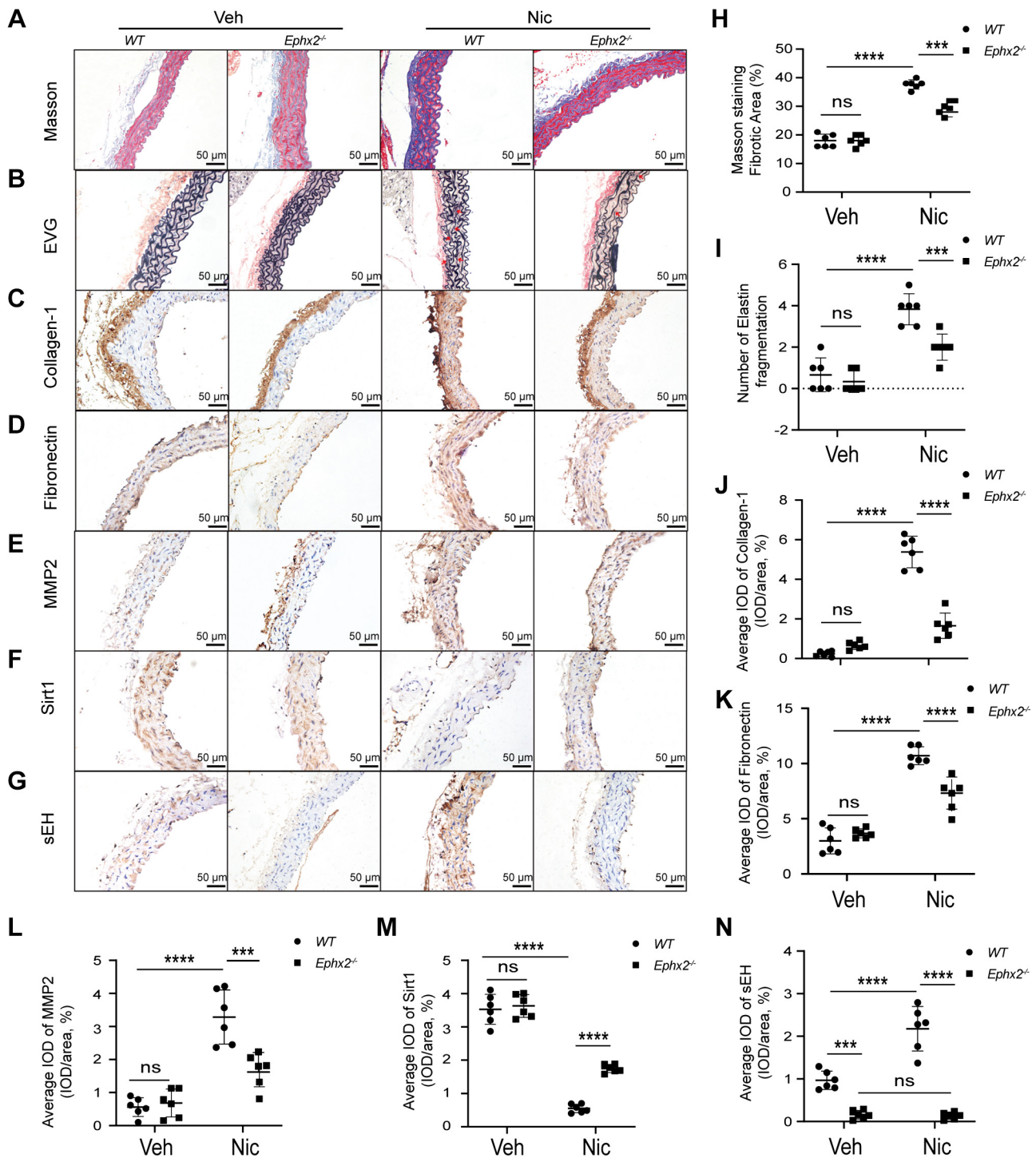
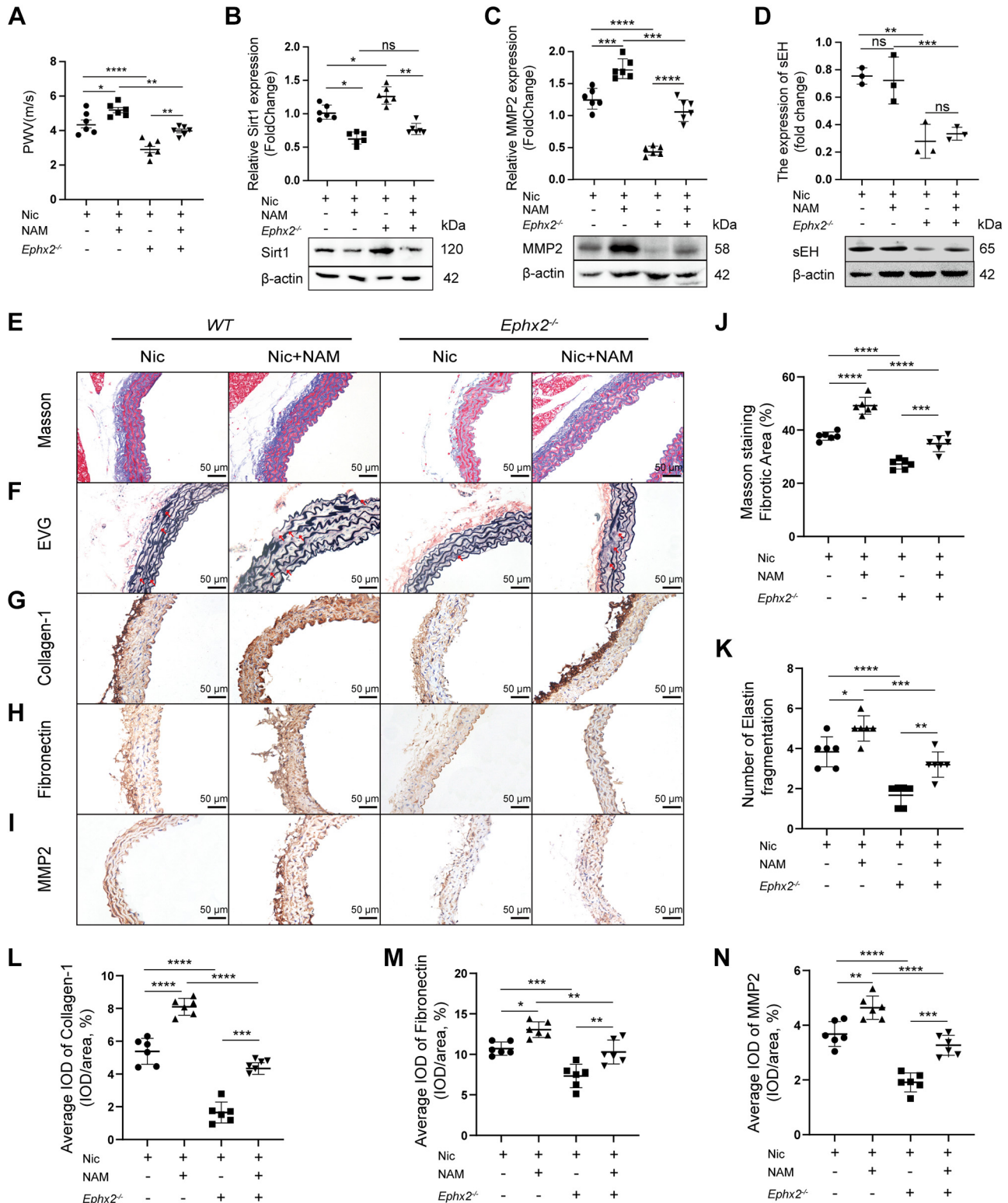


Figure 4. Soluble epoxide hydrolase (sEH) knockout attenuated nicotine-induced extracellular matrix (ECM) remodeling. Representative images (A) and quantification (H) of collagen in aortas were determined by Masson trichrome staining (blue color) ($n = 6$). Representative images (B) and quantification (I) of elastin fragmentation (red arrows) in aortas were determined by Verhoeff's Van Gieson (EVG) staining ($n = 6$). Representative images (C) and quantification (J) of collagen I in aortas were determined by immunohistochemical staining (brown color) ($n = 6$). Representative images (D) and quantification (K) of fibronectin in aortas were determined by immunohistochemical staining (brown color) ($n = 6$). Representative images (E) and quantification (L) of matrix metalloproteinase 2 (MMP2) in aortas were determined by immunohistochemical staining (brown color) ($n = 6$). Representative images (F) and quantification (M) of sirtuin-1 (SIRT1) in aortas were determined by immunohistochemical staining (brown color) ($n = 6$). Representative images (G) and quantification (N) of sEH in aortas were determined by immunohistochemical staining (brown color) ($n = 6$). All data are presented as means \pm SD by two-way ANOVA. *** $P < 0.001$; **** $P < 0.0001$; ns, no significance. Scale bar = 50 μ m.

stiffness, characterized by YAP dephosphorylation and nuclear accumulation. Therefore, we explored whether *Ephx2* knockout affects YAP activation. Phosphorylation of YAP was analyzed by immunoprecipitation and IHC. As shown in Fig. 7, A–D, nicotine markedly decreased the expression of p-YAP (S-127) in aortas of WT mice, which was attenuated in

Ephx2^{−/−} mice. However, SIRT1 inhibition partially reversed the protective effects of *Ephx2* knockout on nicotine-induced p-YAP (S-127) downregulation (Fig. 7, A–D). In addition, the depressive effects of *Ephx2* deletion on nicotine-induced YAP nuclear accumulation were partially abolished by SIRT1 inhibition (Fig. 7E).



To explore the relationship between SIRT1 and YAP, we performed the immunoprecipitation experiment. The immunoprecipitation analysis of YAP in aortas indicated that nicotine treatment markedly increased the acetylation of YAP in WT mice, which was attenuated in *Ephx2*^{-/-} mice (Fig. 7, A and C). In addition, SIRT1 inhibition significantly increased the acetylation of YAP in both WT mice and *Ephx2*^{-/-} mice under nicotine administration (Fig. 7, A and C). These data suggested that *Ephx2* knockout attenuated nicotine-induced YAP activation via SIRT1-mediated deacetylation.

11,12-EET Repressed Nicotine-Induced YAP Activation via SIRT1-Mediated Deacetylation in Vitro

We performed immunoprecipitation experiments to explore the phosphorylation and acetylation of YAP and used immunofluorescence assay to assess the nuclear translocation of YAP in Movas. As expected, 11,12-EET treatment prevented nicotine-induced p-YAP (S-127) downregulation (Fig. 8, A and B) and inhibited YAP activation induced by SIRT1 downregulation-triggered YAP acetylation (Fig. 8, A–D) in Movas. However, these effects were partially reversed in Movas treated with SIRT1 inhibitor (Fig. 8, A–D). Moreover, YAP knockdown markedly attenuated nicotine-induced MMP2 upregulation without affection on SIRT1 expression (Fig. 8E). These data indicated that 11,12-EET repressed nicotine-induced YAP activation via SIRT1-mediated deacetylation.

DISCUSSION

In the present study, we described the protective role of sEH knockout in nicotine-induced vascular stiffness and revealed the potential mechanism. First, we found that nicotine treatment enhanced the sEH expression and activity of aortas in WT mice, resulted in decreased EETs levels in aortas. Second, sEH knockout repressed nicotine-induced vascular stiffness and ECM remodeling, which was partly blocked by SIRT1 inhibition. These results suggest that sEH knockout repressed nicotine-induced arterial stiffness via limiting the loss of SIRT1 (Fig. 9).

Consistent with our conclusion, previous studies demonstrated that *Ephx2* deletion and sEH inhibition attenuated vascular remodeling and arterial stiffness. Dorrance et al. (24) first reported that 12-(3-adamantan-1-yl-ureido)dodecanoic acid (AUDA) treatment caused the vessels from the stroke-prone spontaneously hypertensive rats to be less stiff without any effects on vascular structure, although the mechanisms behind this change were not clear. Furthermore, Simpkins et al. (25) demonstrated that sEH inhibition or *Ephx2* gene deletion antagonized neointimal formation in vivo and they predicted

the beneficial effects of sEH inhibitors on smoking-linked cardiovascular events. In this study, we identified this hypothesis directly and further explored the potential mechanisms.

Nicotine, the main content of cigarettes, is one of the most significant contributors to cardiovascular disease (3). As nicotine is also widely used in nicotine replacement treatment and e-cigarettes, we use nicotine rather than cigarette smoking to induce arterial stiffness, as others have reported (18, 26–28). After 4 wk of nicotine administration, the plasma cotinine levels were markedly increased and were invariable between *Ephx2* deletion and NAM treatment. In addition, *Ephx2* deletion, nicotine, and NAM administration had no significant effects on the expression of CYP2A6 (Supplemental Fig. S1C), which metabolizes nicotine to cotinine in liver (29). These results indicate that the differences between *Ephx2* null mice and WT mice in nicotine-mediated arterial stiffness were not caused by the nicotine concentration variation.

In this study, nicotine treatment markedly increased arterial PWV, elastin fragmentation, and the accumulation of collagen. The results suggested that nicotine only was enough to induce arterial stiffness and ECM remodeling, which was consistent with the data from other reports (18, 30). In addition, nicotine treatment enhanced sEH expression and activation in aortas. Tong et al. (31) showed that the downregulation of smooth muscle Nox4 significantly attenuated aortic stiffness and atherosclerotic lesions by suppressing sEH activity. In this study, sEH knockout repressed nicotine-induced arterial stiffness and ECM remodeling. Moreover, 11,12-EET pretreatment attenuated nicotine-induced MMP2 upregulation in VSMC. Importantly, we demonstrated that *Ephx2* deletion, nicotine, and NAM administration had no significant effects on CYP2C expression (Supplemental Fig. S1D), which highlighted *Ephx2* deletion as the main cause in attenuating nicotine-induced arterial stiffness, and sEH may be a promising therapeutic target for arterial stiffness.

Numerous studies have demonstrated the protective effects of SIRT1 against CVD (18, 20). In this study, we found nicotine-induced sEH upregulation with decreased SIRT1 expression. To explore the relationship between SIRT1 and sEH in nicotine-induced arterial stiffness, we used NAM as a specific inhibitor of SIRT1 and found that continuous NAM administration markedly reduced SIRT1 expression and activity. Consistent with our observation, others also found that NAM administration can depress SIRT1 expression and activity (32, 33). However, Wan et al. (34) found that NAM treatment increased the expression and deacetylating ability of SIRT1 in the liver. In contrast with Wan's study, Mitchell et al. (35) revealed that NAM treatment significantly increased the acetylation in the global protein of mouse liver

Figure 5. SIRT1 inhibition attenuated the protective effects of soluble epoxide hydrolase (sEH) knockout in nicotine-induced arterial stiffness and vascular remodeling. A: analysis of arterial stiffness of abdominal aortas in *Ephx2*^{-/-} mice and wild-type (WT) mice treated with vehicle or nicotine (5 mg/kg/day), accompanied with or without nicotinamide (NAM) (10 mg/kg/day), for 4 wk (*n* = 6). Western Blot analysis and quantification of sirtuin-1 (SIRT1) (B), MMP2 (C), and sEH (D) expression in aortas from *Ephx2*^{-/-} mice and WT mice treated with vehicle or nicotine accompanied with or without NAM for 4 wk (*n* = 6). Representative images (E) and quantification (J) of collagen content in aortas were determined by Masson trichrome staining (blue color) (*n* = 6). Representative images (F) and quantification (K) of elastin fragmentation (red arrows) in aortas were determined by Verhoeff's Van Gieson (EVG) staining (*n* = 6). Representative images (G) and quantification (L) of collagen I in aortas were determined by immunohistochemical staining (brown color) (*n* = 6). Representative images (H) and quantification (M) of fibronectin in aortas were determined by immunohistochemical staining (brown color) (*n* = 6). Representative images (I) and quantification (N) of matrix metalloproteinase 2 (MMP2) in aortas were determined by immunohistochemical staining (brown color) (*n* = 6). All data are presented as means ± SD by one-way ANOVA. **P* < 0.05; ***P* < 0.01; ****P* < 0.001; *****P* < 0.0001; ns, no significance. Scale bar = 50 μm.

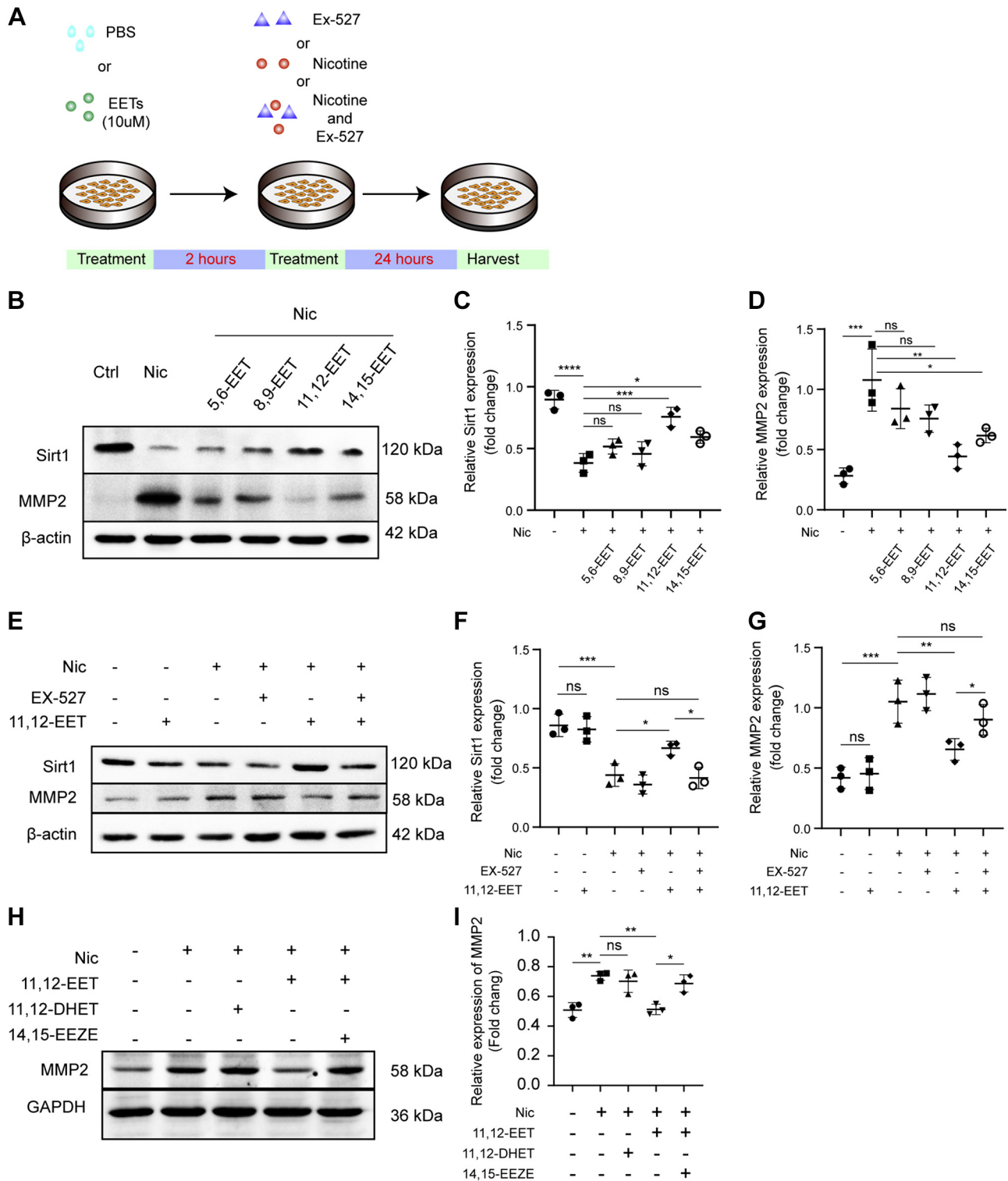


Figure 6. 11,12-EET attenuated nicotine-induced matrix metalloproteinase 2 (MMP2) upregulation via limiting the loss of sirtuin-1 (SIRT1) in vitro. **A:** schematic representation of the Mouse aortic smooth muscle cells (Movas) treatment. Western Blot analysis (**B**) and quantification of SIRT1 (**C**) and MMP2 (**D**) expression in Movas, which were pretreated with or without epoxyeicosatrienoic acids (EETs) (10 μ M) for 2 h, followed by nicotine (1 μ M) treatment for 24 h ($n = 3$). Western Blot analysis (**E**) and quantification of SIRT1 (**F**) and MMP2 (**G**) expression in Movas, which were pretreated with or without 11,12-EET (10 μ M) for 2 h, followed by nicotine (1 μ M) treatment accompanied with or without EX-527 (SIRT1 inhibitor, 10 μ M) treatment for 24 h ($n = 3$). Western Blot analysis (**H**) and quantification (**I**) of MMP2 expression in Movas ($n = 3$). All data are presented as means \pm SD by one-way ANOVA. * $P < 0.05$; ** $P < 0.01$; *** $P < 0.001$; **** $P < 0.0001$; ns, no significance.

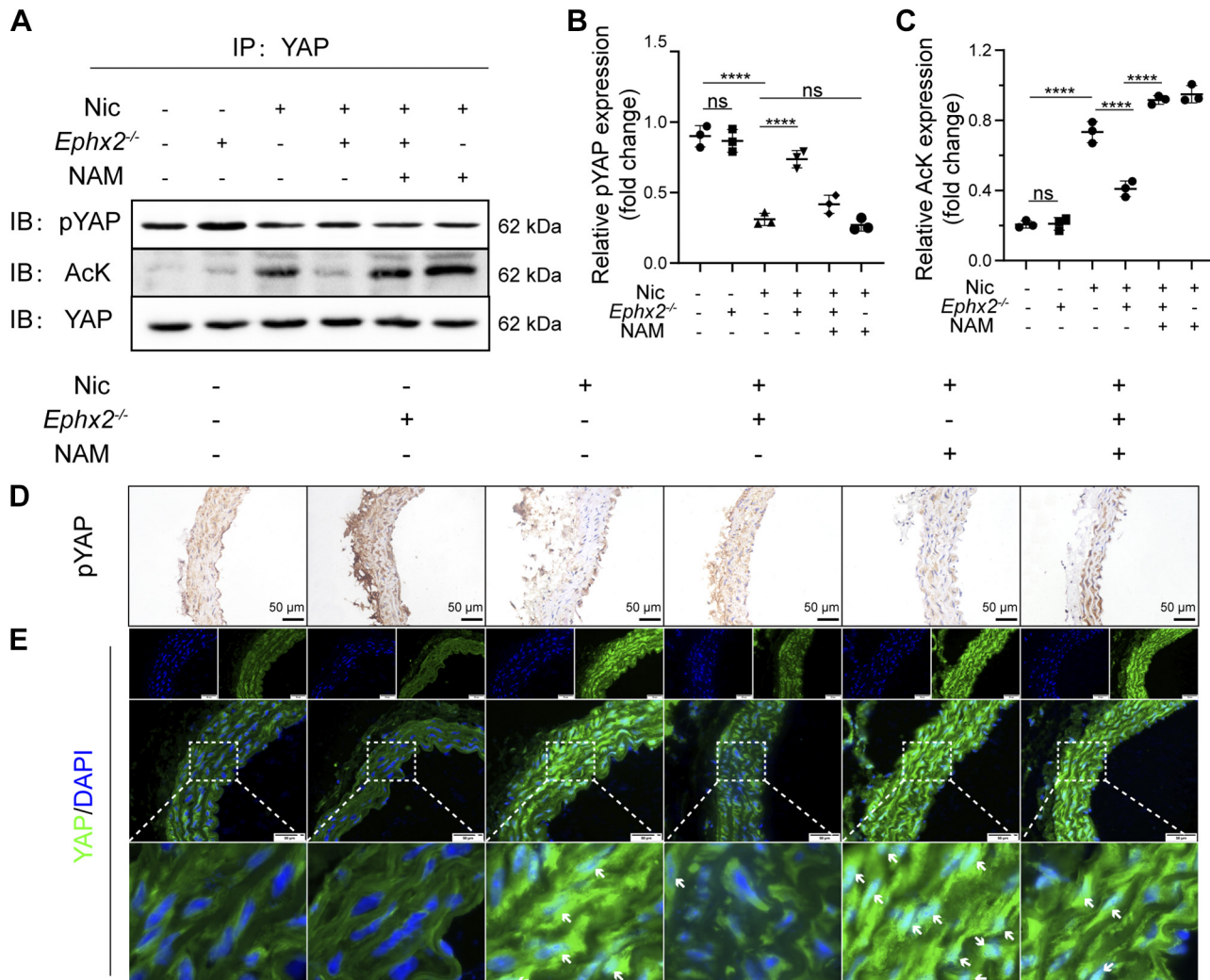


Figure 7. Soluble epoxide hydrolase (sEH) knockout attenuated nicotine-induced yes-associated protein (YAP) activation via sirtuin-1 (SIRT1)-mediated deacetylation. Immunoprecipitation assay (A) showed the phosphorylation at S127 (B) and total acetylation (C) of YAP protein in aortas from *Ephx2*^{-/-} mice and wild-type (WT) mice treated with vehicle or nicotine accompanied with or without nicotinamide (NAM) for 4 wk ($n = 6$). D: the expression of YAP phosphorylation at S127 in aortas was determined by immunohistochemical staining (brown color). E: representative images of immunofluorescence of YAP nuclear translocation (white arrows) in aortas from *Ephx2*^{-/-} mice and WT mice treated with vehicle or nicotine accompanied with or without NAM for 4 wk. All data are presented as means \pm SD by one-way ANOVA. **** $P < 0.0001$; ns, no significance. Scale bar = 50 μ m.

tissues, which indicated that NAM inhibited the deacetylating ability of SIRT1. Taken together, these studies underscore the complex pharmacological profile of NAM; due to the dual action of this compound, acting both as a SIRT1 inhibitor and NAD⁺ precursor. What's more, numerous conditions may cause the controversial results, such as the difference in dose, routes of administration, and animal models.

Decreased SIRT1 expression is widely reported in vascular remodeling and arterial stiffness. Ding et al. (18) described that SIRT1 overexpression attenuated nicotine-induced vascular stiffness. Other studies confirmed the active effects of EETs and EET agonists on SIRT1 activation (36, 37). Consistent with previous studies, we found that nicotine treatment induced SIRT1 downregulation, whereas *Ephx2* deletion and 11,12-EET treatment limited the loss of SIRT1 expression under nicotine administration. Furthermore, SIRT1 inhibition worsen nicotine-induced arterial stiffness and attenuated the protective effects of sEH knockout on

limiting nicotine-induced arterial stiffness. Altogether, these results suggest that sEH knockout prevents the development of nicotine-induced arterial stiffness and ECM remodeling via attenuating the loss of SIRT1 expression. However, the relationship between SIRT1 and EETs in nicotine-induced vascular stiffness remained unknown.

sEH locates in the cytoplasm with hydrolase and phosphatase domains, whereas SIRT1 is a class III protein deacetylase and predominantly locates in the nucleus (8, 14). The differences in localization and function indicate that sEH has hardly any direct contact with SIRT1. In the present study, *Ephx2* deletion or 11,12-EET treatment did not improve the expression or activity of SIRT1 in the groups without nicotine treatment. These results indicate that 11,12-EET is not a direct activator but a potential protector of SIRT1. A recent review (14) summarized the transcriptional regulators of SIRT1, which indicated PPAR α/β as the potential transcriptional regulators of SIRT1. In addition, numerous studies identified the

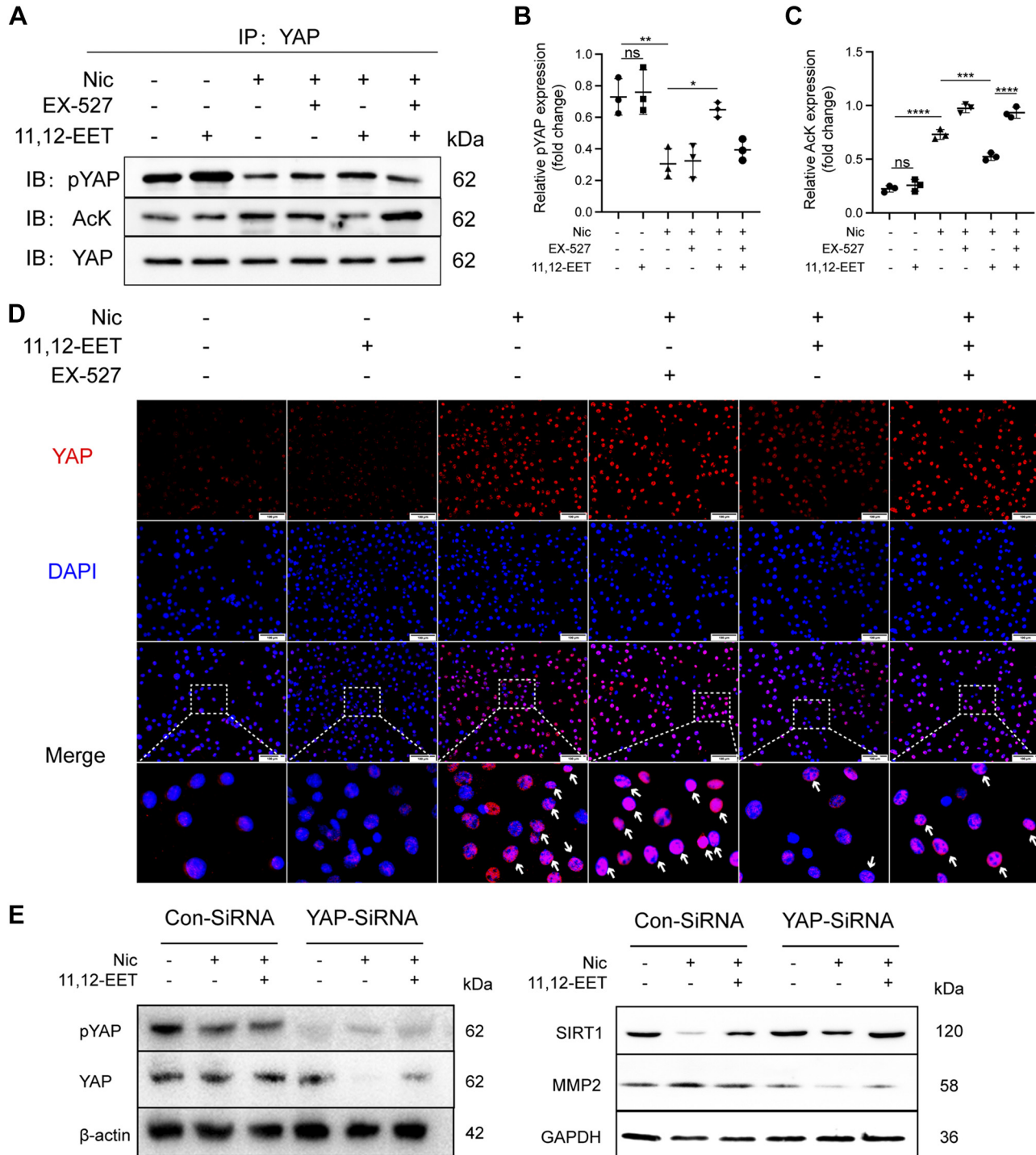


Figure 8. 11,12-EET attenuated nicotine-induced yes-associated protein (YAP) activation via sirtuin-1 (SIRT1)-mediated deacetylation in vitro. Immunoblotting (A) shows the phosphorylation at S127 (B) and total acetylation (AcK) (C) of YAP protein from Mouse aortic smooth muscle cells (Movas) pretreated with or without 11,12-EET (10 μ M) for 2 h, followed by nicotine (1 μ M) treatment accompanied with or without EX-527 (SIRT1 inhibitor, 10 μ M) treatment for 24 h ($n = 3$; *** $P < 0.001$; ** $P < 0.01$; ns, no significance; one-way ANOVA). D: Representative immunofluorescence images of YAP nuclear translocation (white arrows) in movas pretreated with or without 11,12-EET (10 μ M) for 2 h, followed by nicotine (1 μ M) treatment accompanied with or without EX-527 (SIRT1 inhibitor, 10 μ M) treatment for 24 h. E: Western Blot analysis of YAP, pYAP(S127), SIRT1, and matrix metalloproteinase 2 (MMP2) expression in Movas treated with or without siYAP accompanied with or without nicotine and 11,12-EET treatment. All data are presented as means \pm SD by one-way ANOVA. * $P < 0.05$; ** $P < 0.01$; *** $P < 0.001$; **** $P < 0.0001$; ns, no significance. Scale bar = 50 μ m.

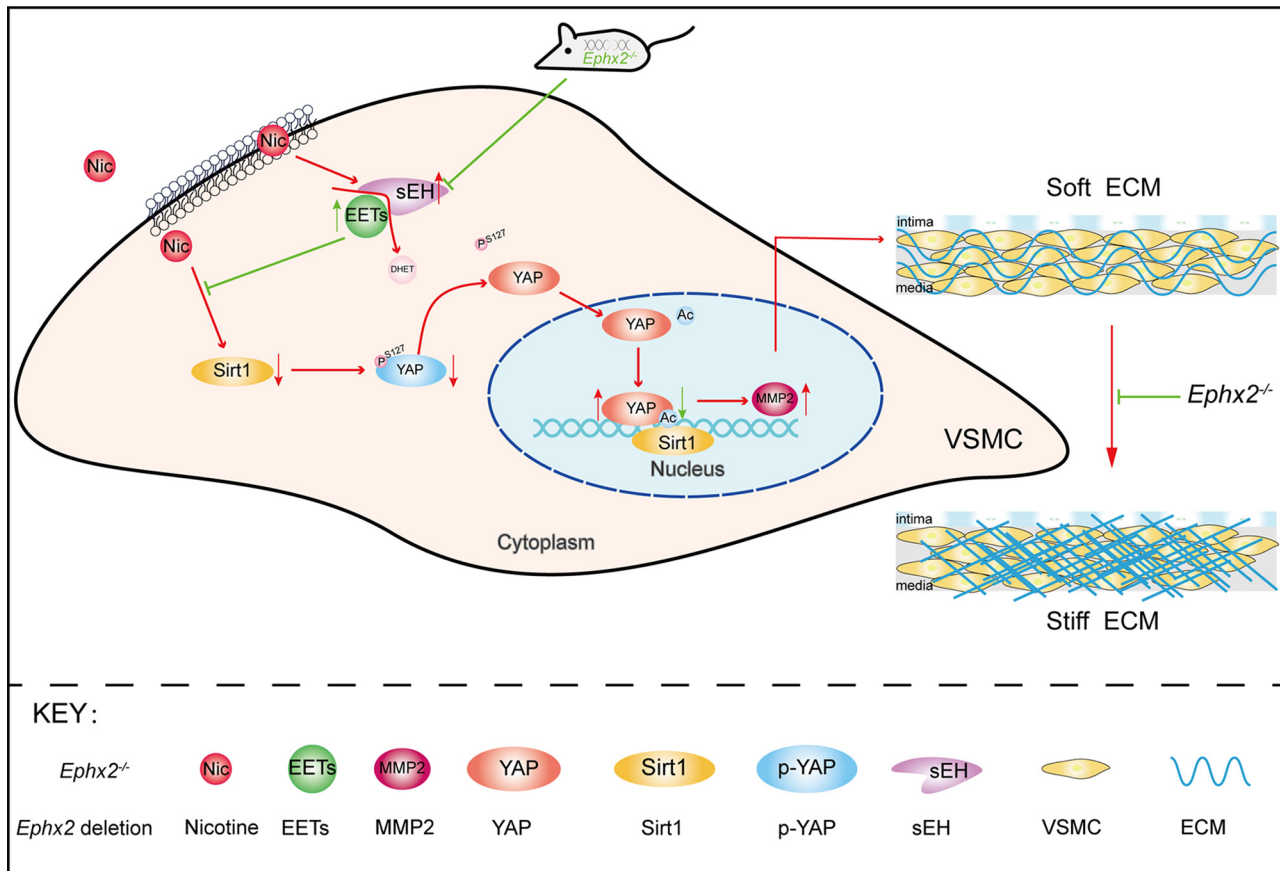


Figure 9. Schematic of soluble epoxide hydrolase (sEH) knockout attenuated nicotine-induced arterial stiffness and extracellular matrix (ECM) remodeling by inhibiting yes-associated protein (YAP) nuclear translocation via limiting the loss of sirtuin-1 (SIRT1).

active effects of sEH inhibitor and EETs on PPAR α/β in vitro and in vivo (38, 39), which indicates PPAR α/β as the potential modulators between EETs and SIRT1, although this was not identified directly.

YAP is found in the cytoplasm and nucleus, and nuclear accumulation is a crucial determinant of its function (40). Abnormal YAP activation causes multiple diseases, including fibrosis, cancer, and atherosclerosis (41). Numerous studies revealed that YAP activation caused vascular remodeling and arterial stiffness (42, 43). Consistent with these observations, we found that nicotine treatment enhanced the nuclear accumulation and acetylation of YAP and resultant arterial stiffness in WT mice, which were attenuated by *Ephx2* deletion. In addition, nicotine treatment decreased YAP phosphorylation in WT mice rather than in *Ephx2*^{-/-} mice. These results indicate that sEH knockout inhibits YAP activation. However, SIRT1 inhibition significantly abolished these effects of sEH knockout, which suggested that sEH knockout attenuated nicotine-induced YAP activation via limiting the loss of SIRT1.

SIRT1, one of NAD⁺-dependent sirtuin deacetylases, targets many nuclear proteins such as transcription regulators (44). Yuan et al. (45) revealed that SIRT1 mediated YAP deacetylation and attenuated YAP activation and nuclear accumulation in atherosclerosis. In our study, SIRT1 inhibition markedly increased YAP acetylation, dephosphorylation, and nuclear translocation. However, the immunoprecipitation

assay indicated that SIRT1 did not coexpressed with pYAP (Supplemental Fig. S4). These results suggest that SIRT1-mediated YAP deacetylation may correlate negatively with YAP nuclear translocation. Furthermore, YAP knockdown by specific siRNA attenuated MMP2 upregulation in nicotine-treated Movas.

In this study, we tested the effects of EETs in cell culture experiments and found that 11,12-EET was the model epoxy-lipid, whereas sEH metabolizes a plethora of epoxides and has a preference for 14,15-EET over 11,12-EET (8). Consistent with our data, others also demonstrated the protective effects of 11,12-EET in smoking-related vascular dysfunction (12). In addition, Zhu et al. (21) found that 11,12-EET stimulation inhibited SIRT1 depression in nicotine-induced vascular remodeling, which indicated that 11,12-EET may be the primary beneficial metabolite (18).

In the present study, we found that NAM didn't completely equilibrate the effects of *Ephx2* deletion on arterial stiffness, which suggested that EETs perform other functions to limit vascular remodeling outside of its effects on SIRT1. It's known that *Ephx2* deletion also has the function of anti-inflammation (46). Smith et al. (47) revealed that sEH inhibition attenuated tobacco smoking-induced lung inflammation, which indicated that anti-inflammation may be another effect of *Ephx2* deletion in attenuating nicotine-induced arterial stiffness. In addition, EETs may also regulate other effectors (such as angiotensin II) to inhibit

vascular remodeling. Numerous studies have demonstrated that nicotine and smoking can significantly activate renin-angiotensin system and cause angiotensin II upregulation, which is associated with endothelial dysfunction and smoking-induced vascular stiffness (48–50). Angiotensin II administration causes sEH upregulation in coronary endothelium, and sEH inhibition and EET analogue decrease angiotensin II-induced hypertension (51–53). These studies suggest that angiotensin II may be the potential effector of EETs in nicotine-induced vascular remodeling as well.

Endothelial dysfunction and VSMC transdifferentiation are decisive progressions in vascular remodeling and stiffness (54–56). Numerous studies indicate that sEH inhibition has protective effects against endothelial dysfunction and VSMC transdifferentiation (31, 57). Although, we found that the inhibitory effect of TPPU (sEH inhibitor) pretreatment on vascular stiffness was a little bit lower than that treated with EETs (unpublished observation, S. Hu, J. Luo, and X. Xu), which indicated that EETs produced by endothelial cells and other organs may also contribute to the inhibitory effect of *Ephx2* deletion in nicotine-induced vascular stiffness. Although numerous reviews underlined the important role of VSMC in vascular remodeling (54, 58), it is still difficult to conclude that specific *Ephx2* deletion in VSMC can reverse vascular remodeling, as sEH was deleted globally in this study. Whether VSMC-specific or endothelial-specific sEH knockout plays a critical role in arterial stiffness remains to be further explored.

There are several limitations in this study. First, as sEH was deleted before nicotine treatment, we only evaluated the prophylactic effects rather than the therapeutic effects. Second, all conclusions in the study were limited to nicotine administration, as cigarette smoking produces numerous substances. Third, it remains unknown whether other toxic effects could explain the effects of sEH knockout on arterial stiffness, as nicotine may have many other toxic effects due to the important role of nACh receptors. In addition, a lot of evidences support that there are sex differences in arterial stiffness and cardiovascular outcomes, and many reviews discussed the sex differences in arterial stiffness (59–61). Furthermore, Mozos et al. (62) revealed the sex differences in smoking-induced arterial stiffness. They found that duration of smoking was associated with increased arterial stiffness independent of sex, whereas a lower exposure to cigarette smoking can increase arterial stiffness in female smokers compared with male smokers, which indicated that females may be more sensitive to the detrimental vascular effects of smoking. But, in a recent study, Ding et al. (18) did not observe the significant difference in arterial stiffness between male and female mice with nicotine treatment. In this study, whether there are sex differences in the effects of sEH knockout on arterial stiffness remains unknown.

In conclusion, our study demonstrated that sEH knockout repressed nicotine-induced arterial stiffness and ECM remodeling via limiting the loss of SIRT1 expression. sEH may be a potential therapeutic target in smoking-induced vascular stiffness.

SUPPLEMENTAL DATA

The supplemental figures and figure legends can be found in the Supplemental Material (<https://doi.org/10.6084/m9.figshare.14566491.v2>).

ACKNOWLEDGMENTS

We thank Dr. Jiankun Yang (Experimental Medicine Research Center of Tongji Hospital, Huazhong University of Science and Technology, China) for technical assistance with histology and Dr. Zheng Wen for instructions on vascular stiffness measurement and analysis.

GRANTS

This work was supported by the Natural Science Foundation of China Grants 81873512 and 81471021.

DISCLOSURES

No conflicts of interest, financial or otherwise, are declared by the authors.

AUTHOR CONTRIBUTIONS

S.H., L.T., and X.X. conceived and designed research; S.H., J.L., M.F., L.L., Y.C., and Y.L. performed experiments; S.H., J.L., M.F., L.L., W.L., R.D., Y.Y., and X.X. analyzed data; S.H., J.L., M.F., and X.X. interpreted results of experiments; S.H., J.L., L.L., Y.C., W.L., R.D., Y.Y., and X.X. prepared figures; S.H. and X.X. drafted manuscript; S.H., J.L., L.T., and X.X. edited and revised manuscript; S.H., J.L., M.F., Y.C., Y.L., R.D., Y.Y., L.T., and X.X. approved final version of manuscript.

REFERENCES

- Ng M, Freeman MK, Fleming TD, Robinson M, Dwyer-Lindgren L, Thomson B, Wollum A, Sanman E, Wulf S, Lopez AD, Murray CJL, Gakidou E. Smoking prevalence and cigarette consumption in 187 countries, 1980–2012. *JAMA* 311: 183–192, 2014. doi:10.1001/jama.2013.284692.
- Caro CG, Parker KH, Lever MJ, Fish PJ. Effect of cigarette smoking on the pattern of arterial blood flow: possible insight into mechanisms underlying the development of arteriosclerosis. *Lancet* 330: 11–13, 1987. doi:10.1016/s0140-6736(87)93052-2.
- Doonan RJ, Hausvater A, Scallan C, Mikhailidis DP, Pilote L, Daskalopoulou SS. The effect of smoking on arterial stiffness. *Hypertens Res* 33: 398–410, 2010. doi:10.1038/hr.2010.25.
- Chirinos JA, Segers P, Hughes T, Townsend R. Large-artery stiffness in health and disease: JACC state-of-the-art review. *J Am Coll Cardiol* 74: 1237–1263, 2019. doi:10.1016/j.jacc.2019.07.012.
- Lyle AN, Raaz U. Killing me softly: causes and mechanisms of arterial stiffness. *Arterioscler Thromb Vasc Biol* 37: e1–e11, 2017. doi:10.1161/ATVBAHA.116.308563.
- Imig JD. Epoxides and soluble epoxide hydrolase in cardiovascular physiology. *Physiol Rev* 92: 101–130, 2012. doi:10.1152/physrev.00021.2011.
- Imig JD. Prospective for cytochrome P450 epoxide hydrolase cardiovascular and renal therapeutics. *Pharmacol Ther* 192: 1–19, 2018. doi:10.1016/j.pharmthera.2018.06.015.
- Imig JD, Hammock BD. Soluble epoxide hydrolase as a therapeutic target for cardiovascular diseases. *Nat Rev Drug Discov* 8: 794–805, 2009. doi:10.1038/nrd2875.
- Wei Q, Doris PA, Pollizotto MV, Boerwinkle E, Jacobs DR, Siscovick DS, Fornage M. Sequence variation in the soluble epoxide hydrolase gene and subclinical coronary atherosclerosis: interaction with cigarette smoking. *Atherosclerosis* 190: 26–34, 2007. doi:10.1016/j.atherosclerosis.2006.02.021.
- Balgoma D, Yang M, Sjodin M, Snowden S, Karimi R, Levanen B, Merikallio H, Kaarteenaho R, Palmberg L, Larsson K, Erle DJ, Dahlen SE, Dahlen B, Skold CM, Wheelock AM, Wheelock CE. Linoleic acid-derived lipid mediators increase in a female-dominated subphenotype of COPD. *Eur Respir J* 47: 1645–1656, 2016. doi:10.1183/13993003.01080-2015.
- Li Y, Yu G, Yuan S, Tan C, Lian P, Fu L, Hou Q, Xu B, Wang H. Cigarette smoke-induced pulmonary inflammation and autophagy

- are attenuated in Ephx2-deficient mice. *Inflammation* 40: 497–510, 2017. doi:10.1007/s10753-016-0495-z.
12. Yang L, Cheriyan J, Gutterman DD, Mayer RJ, Ament Z, Griffin JL, Lazaar AL, Newby DE, Tal-Singer R, Wilkinson IB. Mechanisms of vascular dysfunction in COPD and effects of a novel soluble epoxide hydrolase inhibitor in smokers. *Chest* 151: 555–563, 2017. doi:10.1016/j.chest.2016.10.058.
 13. Liu P-Y, Li Y-H, Chao T-H, Wu H-L, Lin L-J, Tsai L-M, Chen J-H. Synergistic effect of cytochrome P450 epoxigenase CYP2J2*7 polymorphism with smoking on the onset of premature myocardial infarction. *Atherosclerosis* 195: 199–206, 2007. doi:10.1016/j.atherosclerosis.2006.11.001.
 14. Buler M, Andersson U, Hakkola J. Who watches the watchmen? Regulation of the expression and activity of sirtuins. *FASEB J* 30: 3942–3960, 2016. doi:10.1096/fj.201600410RR.
 15. Kane AE, Sinclair DA. Sirtuins and NAD⁺ in the development and treatment of metabolic and cardiovascular diseases. *Circ Res* 123: 868–885, 2018. doi:10.1161/CIRCRESAHA.118.312498.
 16. Winnik S, Auwerx J, Sinclair DA, Matter CM. Protective effects of sirtuins in cardiovascular diseases: from bench to bedside. *Eur Heart J* 36: 3404–3412, 2015. doi:10.1093/eurheartj/ehv290.
 17. D'Onofrio N, Servillo L, Balestrieri ML. SIRT1 and SIRT6 signaling pathways in cardiovascular disease protection. *Antioxid Redox Signal* 28: 711–732, 2018. doi:10.1089/ars.2017.7178.
 18. Ding Y, Han Y, Lu Q, An J, Zhu H, Xie Z, Song P, Zou M-H. Peroxynitrite-mediated SIRT (Sirtuin)-1 inactivation contributes to nicotine-induced arterial stiffness in mice. *Arterioscler Thromb Vasc Biol* 39: 1419–1431, 2019. doi:10.1161/ATVBAHA.118.312346.
 19. Fry JL, Al Sayah L, Weisbrod RM, van Roy I, Weng X, Cohen RA, Bachschmid MM, Seta F. Vascular smooth muscle sirtuin-1 protects against diet-induced aortic stiffness. *Hypertension* 68: 775–784, 2016. doi:10.1161/HYPERTENSIONAHA.116.07622.
 20. Gao D, Zuo Z, Tian J, Ali Q, Lin Y, Lei H, Sun Z. Activation of SIRT1 attenuates Klotho deficiency-induced arterial stiffness and hypertension by enhancing AMP-activated protein kinase activity. *Hypertension* 68: 1191–1199, 2016. doi:10.1161/HYPERTENSIONAHA.116.07709.
 21. Zhu Y, Ding A, Yang D, Cui T, Yang H, Zhang H, Wang C. CYP2J2-produced epoxyeicosatrienoic acids attenuate ischemia/reperfusion-induced acute kidney injury by activating the SIRT1-FoxO3a pathway. *Life Sci* 246: 117327, 2020. doi:10.1016/j.lfs.2020.117327.
 22. Thomas CE, Wang R, Adams-Haduch J, Murphy SE, Ueland PM, Middtun Ø, Brennan P, Johansson M, Gao Y-T, Yuan J-M. Urinary cotinine is as good a biomarker as serum cotinine for cigarette smoking exposure and lung cancer risk prediction. *Cancer Epidemiol Biomarkers Prev* 29: 127–132, 2020. doi:10.1158/1055-9965.EPI-19-0653.
 23. Xie J, Hu D, Wang X, Luo Y, Wang J. Smoking state determined by cotinine and arterial stiffness. *Circ J* 73: 1537–1542, 2009. doi:10.1253/circj.CJ-08-1158.
 24. Dorrance AM, Rupp N, Pollock DM, Newman JW, Hammock BD, Imig JD. An epoxide hydrolase inhibitor, 12-(3-adamantan-1-yl-ureido)dodecanoic acid (AUDA), reduces ischemic cerebral infarct size in stroke-prone spontaneously hypertensive rats. *J Cardiovasc Pharmacol* 46: 842–848, 2005. doi:10.1097/01.fjc.0000189600.74157.6d.
 25. Simpkins AN, Rudic RD, Roy S, Tsai HJ, Hammock BD, Imig JD. Soluble epoxide hydrolase inhibition modulates vascular remodeling. *Am J Physiol Heart Circ Physiol* 298: H795–H806, 2010. doi:10.1152/ajpheart.00543.2009.
 26. Fetterman JL, Keith RJ, Palmisano JN, McGlasson KL, Weisbrod RM, Majid S, Bastin R, Stathos MM, Stokes AC, Robertson RM, Bhatnagar A, Hamburg NM. Alterations in vascular function associated with the use of combustible and electronic cigarettes. *J Am Heart Assoc* 9: e014570, 2020. doi:10.1161/JAHA.119.014570.
 27. Wang Z, Liu B, Zhu J, Di W, Wang Y. Nicotine-mediated autophagy of vascular smooth muscle cell accelerates atherosclerosis via nAChRs/ROS/NF- κ B signaling pathway. *Atherosclerosis* 284: 1–10, 2019. doi:10.1016/j.atherosclerosis.2019.02.008.
 28. Zhu J, Liu B, Wang Z, Di W, Ni H, Zhang L, Wang Y. Exosomes from nicotine-stimulated macrophages accelerate atherosclerosis through miR-21-3p/PTEN-mediated VSMC migration and proliferation. *Theranostics* 9: 6901–6919, 2019. doi:10.7150/thno.37357.
 29. Benowitz NL. Pharmacology of nicotine: addiction, smoking-induced disease, and therapeutics. *Annu Rev Pharmacol Toxicol* 49: 57–71, 2009. doi:10.1146/annurev.pharmtox.48.113006.094742.
 30. Wagenhäuser MU, Schellinger IN, Yoshino T, Toyama K, Kayama Y, Deng A, Guenther SP, Petzold A, Mulorz J, Mulorz P, Hasenfuß G, Ibing W, Elvers M, Schuster A, Ramasubramanian AK, Adam M, Schelzig H, Spin JM, Raaz U, Tsao PS. Chronic nicotine exposure induces murine aortic remodeling and stiffness segmentation-implications for abdominal aortic aneurysm susceptibility. *Front Physiol* 9: 1459, 2018. doi:10.3389/fphys.2018.01459.
 31. Tong X, Khandelwal AR, Wu X, Xu Z, Yu W, Chen C, Zhao W, Yang J, Qin Z, Weisbrod RM, Seta F, Ago T, Lee KSS, Hammock BD, Sadoshima J, Cohen RA, Zeng C. Pro-atherogenic role of smooth muscle Nox4-based NADPH oxidase. *J Mol Cell Cardiol* 92: 30–40, 2016. doi:10.1016/j.yjmcc.2016.01.020.
 32. Li D, Wang X, Huang Q, Li S, Zhou Y, Li Z. Cardioprotection of CAPE-oNO₂ against myocardial ischemia/reperfusion induced ROS generation via regulating the SIRT1/eNOS/NF- κ B pathway in vivo and in vitro. *Redox Biol* 15: 62–73, 2018. doi:10.1016/j.redox.2017.11.023.
 33. Liu Z, Gan L, Liu G, Chen Y, Wu T, Feng F, Sun C. Sirt1 decreased adipose inflammation by interacting with Akt2 and inhibiting mTOR/S6K1 pathway in mice. *J Lipid Res* 57: 1373–1381, 2016. doi:10.1194/jlr.M063537.
 34. Wan H-F, Li J-X, Liao H-T, Liao M-H, Luo L, Xu L, Yuan K-F, Zeng Y. Nicotinamide induces liver regeneration and improves liver function by activating SIRT1. *Mol Med Report* 19: 555–562, 2018. doi:10.3892/mmr.2018.9688.
 35. Mitchell SJ, Bernier M, Aon MA, Cortassa S, Kim EY, Fang EF, Palacios HH, Ali A, Navas-Enamorado I, Di Francesco A, Kaiser TA, Waltz TB, Zhang N, Ellis JL, Elliott PJ, Frederick DW, Bohr VA, Schmidt MS, Brenner C, Sinclair DA, Sauve AA, Baur JA, Cabo R. Nicotinamide improves aspects of healthspan, but not lifespan, in mice. *Cell Metab* 27: 667–676.e4, 2018. doi:10.1016/j.cmet.2018.02.001.
 36. El-Sikhry HE, Alsaleh N, Dakarapu R, Falck JR, Seubert JM. Novel roles of epoxyeicosanoids in regulating cardiac mitochondria. *PLoS One* 11: e0160380, 2016. doi:10.1371/journal.pone.0160380.
 37. Raffaele M, Bellner L, Singh SP, Favero G, Rezzani R, Rodella LF, Falck JR, Abraham NG, Vanella L. Epoxyeicosatrienoic intervention improves NAFLD in leptin receptor deficient mice by an increase in PGC1 α -HO-1-PGC1 α -mitochondrial signaling. *Exp Cell Res* 380: 180–187, 2019. doi:10.1016/j.yexcr.2019.04.029.
 38. Spector AA, Norris AW. Action of epoxyeicosatrienoic acids on cellular function. *Am J Physiol Cell Physiol* 292: C996–C1012, 2007. doi:10.1152/ajpcell.00402.2006.
 39. Wang X, Li L, Wang H, Xiao F, Ning Q. Epoxyeicosatrienoic acids alleviate methionine-choline-deficient diet-induced non-alcoholic steatohepatitis in mice. *Scand J Immunol* 90: e12791, 2019. doi:10.1111/sji.12791.
 40. Piccolo S, Dupont S, Cordenonsi M. The biology of YAP/TAZ: hippo signaling and beyond. *Physiol Rev* 94: 1287–1312, 2014. doi:10.1152/physrev.00005.2014.
 41. Totaro A, Panciera T, Piccolo S. YAP/TAZ upstream signals and downstream responses. *Nat Cell Biol* 20: 888–899, 2018. doi:10.1038/s41556-018-0142-z.
 42. Bertero T, Oldham WM, Cottrill KA, Pisano S, Vanderpool RR, Yu Q, Zhao J, Tai Y, Tang Y, Zhang Y-Y, Rehman S, Sugahara M, Qi Z, Gorscan J 3rd, Vargas SO, Saggat R, Saggat R, Wallace WD, Ross DJ, Haley KJ, Waxman AB, Parikh VN, De Marco T, Hsue PV, Morris A, Simon MA, Norris KA, Gaggioli C, Loscalzo J, Fessel J, Chan S. Vascular stiffness mechanoactivates YAP/TAZ-dependent glutaminolysis to drive pulmonary hypertension. *J Clin Invest* 126: 3313–3335, 2016. doi:10.1172/JCI86387.
 43. Calvo F, Ege N, Grande-Garcia A, Hooper S, Jenkins RP, Chaudhry SI, Harrington K, Williamson P, Moendarbary E, Charras G, Sahai E. Mechanotransduction and YAP-dependent matrix remodelling is required for the generation and maintenance of cancer-associated fibroblasts. *Nat Cell Biol* 15: 637–646, 2013. doi:10.1038/ncb2756.
 44. Narita T, Weinert BT, Choudhary C. Functions and mechanisms of non-histone protein acetylation. *Nat Rev Mol Cell Biol* 20: 156–174, 2019 [Erratum in *Nat Rev Mol Cell Biol* 20: 508]. doi:10.1038/s41580-018-0081-3.

45. Yuan P, Hu Q, He X, Long Y, Song X, Wu F, He Y, Zhou X. Laminar flow inhibits the Hippo/YAP pathway via autophagy and SIRT1-mediated deacetylation against atherosclerosis. *Cell death Dis* 11: 141, 2020. doi:10.1038/s41419-020-2343-1.
46. Morisseau C, Hammock BD. Impact of soluble epoxide hydrolase and epoxyeicosanoids on human health. *Annu Rev Pharmacol Toxicol* 53: 37–58, 2013. doi:10.1146/annurev-pharmtox-011112-140244.
47. Smith KR, Pinkerton KE, Watanabe T, Pedersen TL, Ma SJ, Hammock BD. Attenuation of tobacco smoke-induced lung inflammation by treatment with a soluble epoxide hydrolase inhibitor. *Proc Natl Acad Sci USA* 102: 2186–2191, 2005. doi:10.1073/pnas.0409591102.
48. Oakes JM, Fuchs RM, Gardner JD, Lazartigues E, Yue X. Nicotine and the renin-angiotensin system. *Am J Physiol Regul Integr Comp Physiol* 315: R895–R906, 2018. doi:10.1152/ajpregu.00099.2018.
49. Vasconez AE, Janetzko P, Oo JA, Pflüger-Müller B, Ratiu C, Gu L, Helin K, Geisslinger G, Fleming I, Schröder K, Fork C, Brandes RP, Leisegang MS. The histone demethylase Jarid1b mediates angiotensin II-induced endothelial dysfunction by controlling the 3'UTR of soluble epoxide hydrolase. *Acta Physiol (Oxf)* 225: e13168, 2019. doi:10.1111/apha.13168.
50. Yuan Y-M, Luo L, Guo Z, Yang M, Ye R-S, Luo C. Activation of renin-angiotensin-aldosterone system (RAAS) in the lung of smoking-induced pulmonary arterial hypertension (PAH) rats. *J Renin Angiotensin Aldosterone Syst* 16: 249–253, 2015. doi:10.1177/1470320315576256.
51. Hye Khan MA, Pavlov TS, Christain SV, Neckárö J, Staruschenko A, Gauthier KM, Capdevila JH, Falck JR, Campbell WB, Imig JD. Epoxyeicosatrienoic acid analogue lowers blood pressure through vasodilation and sodium channel inhibition. *Clin Sci (Lond)* 127: 463–474, 2014. doi:10.1042/CS20130479.
52. Jung O, Brandes RP, Kim I-H, Schweda F, Schmidt R, Hammock BD, Busse R, Fleming I. Soluble epoxide hydrolase is a main effector of angiotensin II-induced hypertension. *Hypertension* 45: 759–765, 2005. doi:10.1161/01.HYP.0000153792.29478.1d.
53. Mak S-K, Yu C-M, Sun W-T, He G-W, Liu X-C, Yang Q. Tetramethylpyrazine suppresses angiotensin II-induced soluble epoxide hydrolase expression in coronary endothelium via anti-ER stress mechanism. *Toxicol Appl Pharmacol* 336: 84–93, 2017. doi:10.1016/j.taap.2017.10.016.
54. Lacolley P, Regnault V, Segers P, Laurent S. Vascular smooth muscle cells and arterial stiffening: relevance in development, aging, and disease. *Physiol Rev* 97: 1555–1617, 2017. doi:10.1152/physrev.00003.2017.
55. Marti CN, Gheorghiade M, Kalogeropoulos AP, Georgiopoulou VV, Quyyumi AA, Butler J. Endothelial dysfunction, arterial stiffness, and heart failure. *J Am Coll Cardiol* 60: 1455–1469, 2012. doi:10.1016/j.jacc.2011.11.082.
56. van den Bergh G, Opdebeeck B, D'Haese PC, Verhulst A. The vicious cycle of arterial stiffness and arterial media calcification. *Trends Mol Med* 25: 1133–1146, 2019. doi:10.1016/j.molmed.2019.08.006.
57. Bellien J, Joannides R, Richard V, Thuillez C. Modulation of cytochrome-derived epoxyeicosatrienoic acids pathway: a promising pharmacological approach to prevent endothelial dysfunction in cardiovascular diseases? *Pharmacol Ther* 131: 1–17, 2011. doi:10.1016/j.pharmthera.2011.03.015.
58. Sehgel NL, Vatner SF, Meininger GA. "Smooth muscle cell stiffness syndrome"-revisiting the structural basis of arterial stiffness. *Front Physiol* 6: 335, 2015. doi:10.3389/fphys.2015.00335.
59. DuPont JJ, Kenney RM, Patel AR, Jaffe IZ. Sex differences in mechanisms of arterial stiffness. *Br J Pharmacol* 176: 4208–4225, 2019. doi:10.1111/bph.14624.
60. Ogola BO, Zimmerman MA, Clark GL, Abshire CM, Gentry KM, Miller KS, Lindsey SH. New insights into arterial stiffening: does sex matter? *Am J Physiol Heart Circ Physiol* 315: H1073–H1087, 2018. doi:10.1152/ajpheart.00132.2018.
61. Rossi P, Francès Y, Kingwell BA, Ahimastos AA. Gender differences in artery wall biomechanical properties throughout life. *J Hypertens* 29: 1023–1033, 2011. doi:10.1097/HJH.0b013e328344da5e.
62. Mozos I, Maidana JP, Stoian D, Stehlik M. Gender differences of arterial stiffness and arterial age in smokers. *IJERPH* 14: 565, 2017. doi:10.3390/ijerph14060565.